Water lines interfering with the A-band are poorly characterized and Brian Drouin has worked on the O2 A band

S. Vasilchenko, S.N. N Mikhailenko, A. Campargue

Journal of Quantitative Spectroscopy and Radiative Transfer

Water vapor absorption in the region of the oxygen A-band near 760 nm

--Manuscript Draft--

Manuscript Number:	
Article Type:	VSI:HITRAN2020
Keywords:	water vapor; H2O; absorption spectroscopy; rovibrational energy level; oxygen A band
Corresponding Author:	alain Campargue cnrs Saint Martin d'Hères, France
First Author:	Semen Vasilchenko
Order of Authors:	Semen Vasilchenko
	Semen Mikhailenko
	alain Campargue
Abstract:	The oxygen A-band near 760 nm is used to determine the air-mass along the line of sight from ground or space borne atmospheric spectra. This band is located in a spectral region of very weak absorption of water vapor. The increased requirements on the determination of the air columns make suitable to accurately characterize water absorption spectrum in the region. In the present work, we use cavity ring down spectroscopy (CRDS) to measure with unprecedented sensitivity and accuracy the water spectrum in the 12969 - 13172 cm-1 region. While about fifty transitions were previously detected in the region, a total of about 580 water lines are measured by CRDS and rovibrationally assigned, leading to the determination of 103 new levels and correction of 135 levels of H216O. Spectroscopic line lists available in the region - HITRAN, W2020 and theoretical line lists - show some important deviations compared to observations. In particular, line intensities are poorly predicted by available ab initio calculations for transitions involving a highly bending excitation.
Suggested Reviewers:	Nikolai Zobov zobov@ipfran.ru
	Keeyoon Sung Keeyoon.Sung@jpl.nasa.gov
	Vivienne Payne vivienne.h.payne@jpl.nasa.gov Water lines interfering with the A-band are poorly characterized and Vivienne Payne is involved in OCO mission who is using the A band of oxygen
	Brian Drouin brian.j.drouin@jpl.nasa.gov Water lines interfering with the A-band are poorly characterized and Brian Drouin has worked on the O2 A band
	Eamon Conway eamon.conway@cfa.harvard.edu

Cover Letter

Dear Sir,
Please find attached the paper:
Water vapor absorption in the region of the oxygen A-band near 760 nm

S. Vasilchenko, S.N. Mikhailenko, A. Campargue

that we submit as article in the JQSRT

Regards,
Alain Campargue

Highlights

- High sensitivity absorption spectra of water vapor in the region of the A-band of oxygen near 760 nm
- About 600 water lines are measured rovibrationally assigned between 12969 and 13170 cm^{-1}
- The detection threshold corresponds to line intensities smaller than to 1×10^{-29} cm/molecule.
- 103 upper energy levels of $H_2{}^{16}O$ are newly determined and 135 energy levels are corrected
- A line list of 693 transitions of $H_2{}^{16}O$, $H_2{}^{18}O$ and $HD^{16}O$ is recommended for the considered region.

Graphical Abstract

Click here to access/download;Graphical Abstract;Graph abstract.jpg

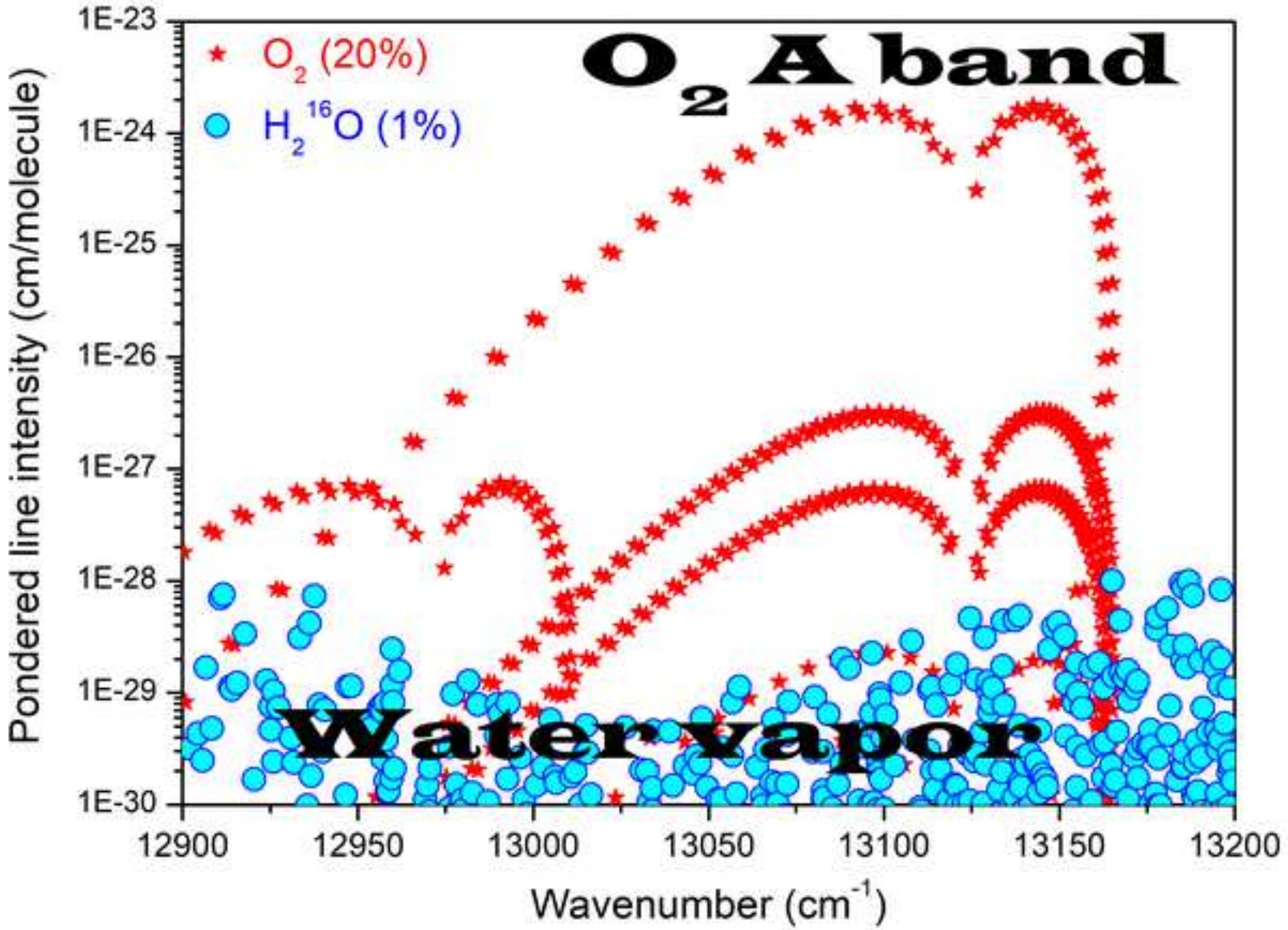

Water vapor absorption in the region of the oxygen A-band near 760 nm

S. Vasilchenko [a], S.N. Mikhailenko [a,b], A. Campargue [c*],

[a] *V.E. Zuev Institute of Atmospheric Optics, SB, Russian Academy of Science, 1, Academician Zuev square, 634055 Tomsk, Russia*
[b] *Climate and Environmental Physics Laboratory, Ural Federal University, 19, Mira av., 620002 Yekaterinburg, Russia*
[c] *Univ. Grenoble Alpes, CNRS, LIPhy, 38000 Grenoble, France*

Key words: water vapor; H_2O; absorption spectroscopy; rovibrational energy level; oxygen A band

Number of Pages: 25
Number of Figures: 9
Number of Tables: 2

Corresponding author.
E-mail address: Alain.Campargue@univ-grenoble-alpes.fr
Tel.: 33 4 76 51 43 19 Fax. 33 4 76 63 54 95

Abstract

The oxygen A-band near 760 nm is used to determine the air-mass along the line of sight from ground or space borne atmospheric spectra. This band is located in a spectral region of very weak absorption of water vapor. The increased requirements on the determination of the air columns make suitable to accurately characterize water absorption spectrum in the region. In the present work, we use cavity ring down spectroscopy (CRDS) to measure with unprecedented sensitivity and accuracy the water spectrum in the 12969 - 13172 cm^{-1} region. While about fifty transitions were previously detected in the region, a total of about 580 water lines are measured by CRDS and rovibrationally assigned, leading to the determination of 103 new levels and correction of 135 levels of $H_2{}^{16}O$. Spectroscopic line lists available in the region - HITRAN, W2020 and theoretical line lists - show some important deviations compared to observations. In particular, line intensities are poorly predicted by available *ab initio* calculations for transitions involving a highly bending excitation.

1. Introduction

As the mixing ratio of oxygen is constant in the Earth's atmosphere (0.2095 according to Ref. [1]), the A-band of O_2 is largely used to determine the air-mass along the line of sight from ground or space borne atmospheric spectra in particular for remote sensing calibration [2-4]. The accuracy of the derived dry air column has a direct impact on the column mole fraction of the targeted species (CO_2, CH_4, CO etc…). In this context, the possible contribution of absorption lines of atmospheric water in the region of the O_2 A-band near 760 nm has to be considered as a possible bias on the air-mass retrieval. According to the HITRAN [5] and GEISA [6] spectroscopic databases, the A-band corresponds to a spectral region of weak absorption of water vapor. Taking into account rough atmospheric abundance values of 20% and 1% for oxygen and water vapor, respectively, the strongest water lines represents no more than 0.1 and 0.01% of the strongest oxygen lines near 13000 and 13100 cm^{-1}, respectively (see **Fig. 1**). The impact of water absorption is thus expected to be very small. Nevertheless, due to the scarcity of previous measurements in the region, line parameters provided by spectroscopic database should be tested. In particular, line intensities are mostly calculated values which have a questionable accuracy in this high energy range (the HITRAN code for the intensity error bar of most of the lines in the region corresponds to >20%).

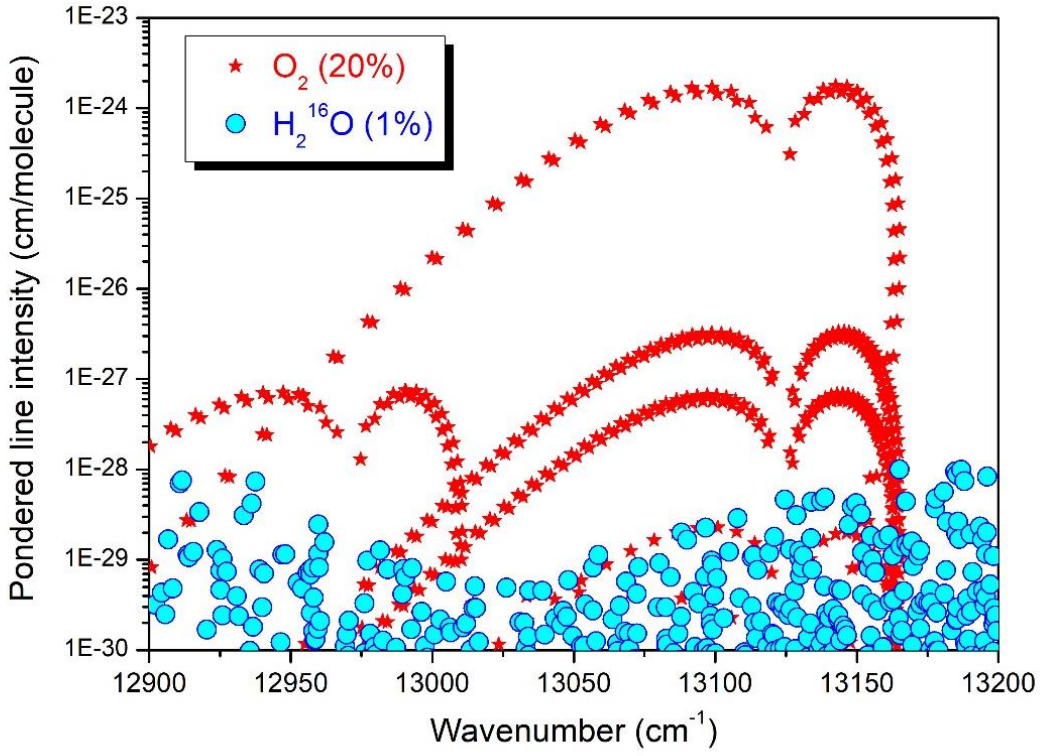

Fig. 1

Overview of the HITRAN2016 line lists of oxygen (red stars) and water vapour (blue circles) in the region of the O_2 A-band. Line intensities have been multiplied by 20% and 1% in order to roughly account for the atmospheric abundances of oxygen and water vapor, respectively.

The characterization of water lines in the region requires high sensitivity techniques. A review of experimental studies between 12900 and 13500 cm^{-1}, up to 2008, was included in Ref. [7] (see Fig. 11 of this reference). To the best of our knowledge, no new high sensitivity measurements have been published in the region since that date except our CRDS study in the 13312-13378 cm^{-1} interval, thus above the A-band region. The sensitivity of the Fourier transform spectroscopy (FTS) technique coupled with multi reflection cell providing absorption pathlength of several hundred meters is not sufficient for reliable detection of water absorption lines in the A-band region (see below) [8-13]. The most sensitive investigation in the region was performed by intracavity laser spectroscopy (ICLAS) between 12746 and 13558 cm^{-1} [7]. This laser technique is a quantitative technique with effective absorption pathlength of several tens km giving access to absorption coefficients as low as $\alpha_{min} \sim 10^{-9}$ cm^{-1} [14]. About fifty lines could be measured by ICLAS in the A-band region (12969-13172 cm^{-1}) above an intensity threshold of about 10^{-27} cm/molecule [7]. The spectral resolution of the ICLAS spectra which is fixed by the apparatus function of a grating spectrograph limits the accuracy of ICLAS intensity values to 5-10% in favourable cases [14]. As described below, the sensitivity of the present CRDS recordings ($\alpha_{min} \sim 5\times10^{-11}$ cm^{-1}) allows for lowering the detectivity threshold to about 10^{-29} cm/molecule and increasing the number of detected lines to about 580.

The rest of the report is organized as follows. The CRDS spectrometer developed at the Institute of Atmospheric Optics (Tomsk) and the line list construction are presented in the next Section 2. Section 3 includes the vibration-rotation assignments performed using known experimental energy levels and calculated water spectra based on variational calculations by Schwenke and Partridge (SP) [15-17]. As a result of the high sensitivity of the spectra, in addition to the $H_2{}^{16}O$ lines, some lines of the $HD^{16}O$ and $H_2{}^{18}O$ isotopologues in "natural" isotopic abundance could be identified. Section 4 is devoted to a comparison to the previous ICLAS study [7], to the HITRAN2016 list and to recent W2020 lists of $H_2{}^{16}O$ and $H_2{}^{18}O$ with line positions derived from empirically determined energy levels [18].

2. Experiment

Figure 2 shows the block diagram of the experimental setup. The experimental arrangement is very similar to that described in details in Refs. [19,20]. Briefly, the CRDS spectrometer consists of a steel tube 1.4 m long and 10 mm inner diameter and fitted with two high reflectivity mirrors (from Layertec, reflectivity better than 99.99% throughout the laser tuning range). The two spherical mirrors (0.5-inch diameter, 1 m radius of curvature) are supported by adjustable frames which are force fit on the steel body of the cell through rubber seals. An external cavity diode laser (ECDL) from Sacher Lasertechnik, tunable in the 745–775 nm spectral range (12900–13400 cm^{-1}) is used as radiation source. The delivered radiation power varies from 33 to 40 mW depending on the wavelength. The laser is equipped with an optical insulator to eliminate the optical feedback and a fiber optic port; the output power of the single-mode fiber ranges between 18 and 24 mW. Coarse laser tuning is provided by rotating the diffraction grating of the cavity, and precise tuning, by the voltage across the piezoelectric

element of the diffraction grating or by the laser diode current. The laser line width is ~100 kHz over a 1 ms integration time *i.e.* more than one order of magnitude better than that of DFB laser diodes common, for the CRDS technique. This provides better spectrometer sensitivity due to more efficient radiation injection into the cavity and smaller frequency fluctuations. A fiber-optic beam splitter directs 20% of the radiation to a wavelength meter (HighFinesse WSU, 5 MHz resolution, measurement frequency up to 400 Hz). The remaining 80% is directed to an fiber-optic acousto-optical modulator (from AAOptoelectronics) controlled by an 80-MHz driver (RF generator), which interrupts the radiation input into the cavity in 60 ns. To obtain resonance between the longitudinal mode of the cavity and a laser beam, the output mirror of the cavity is mounted on a tubular piezoelectric element, to which a saw tooth voltage is applied. At the cavity output, the radiation is focused onto a silicon avalanche photodetector (Thorlabs APD410A). When resonance occurs, the radiation input into the cavity is interrupted by the acousto-optical modulator upon a photodiode signal attain a certain voltage threshold, and the exponential decay of the intracavity field (ring-down) is recorded. Data are collected by an NI-PCIe 6259 I/O board (16 bit resolution, acquisition frequency 1 M samples per second); the system is controlled and data are processed by a dedicated Labview software.

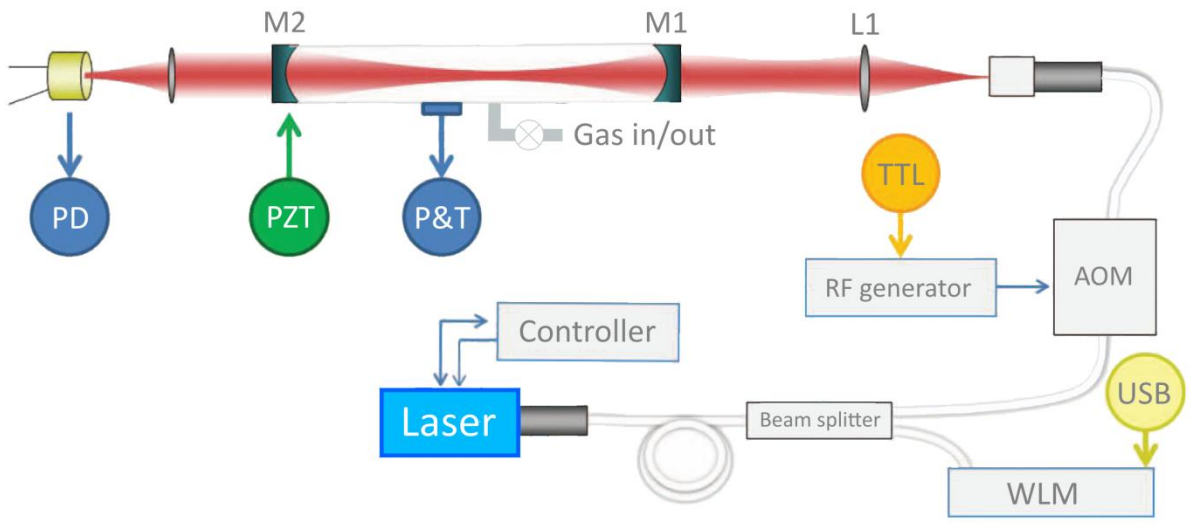

Fig. 2

Experimental setup: wavelength meter (WLM), radio-frequency generator (RF generator), acousto-optical modulator (AOM), transistor-transistor logic switch of RF generator (TTL), matching lens (L1), high reflectivity mirrors (M1 and M2), piezoelectric transducer (PZT), pressure and temperature sensors (P&T), and photodiode (PD).

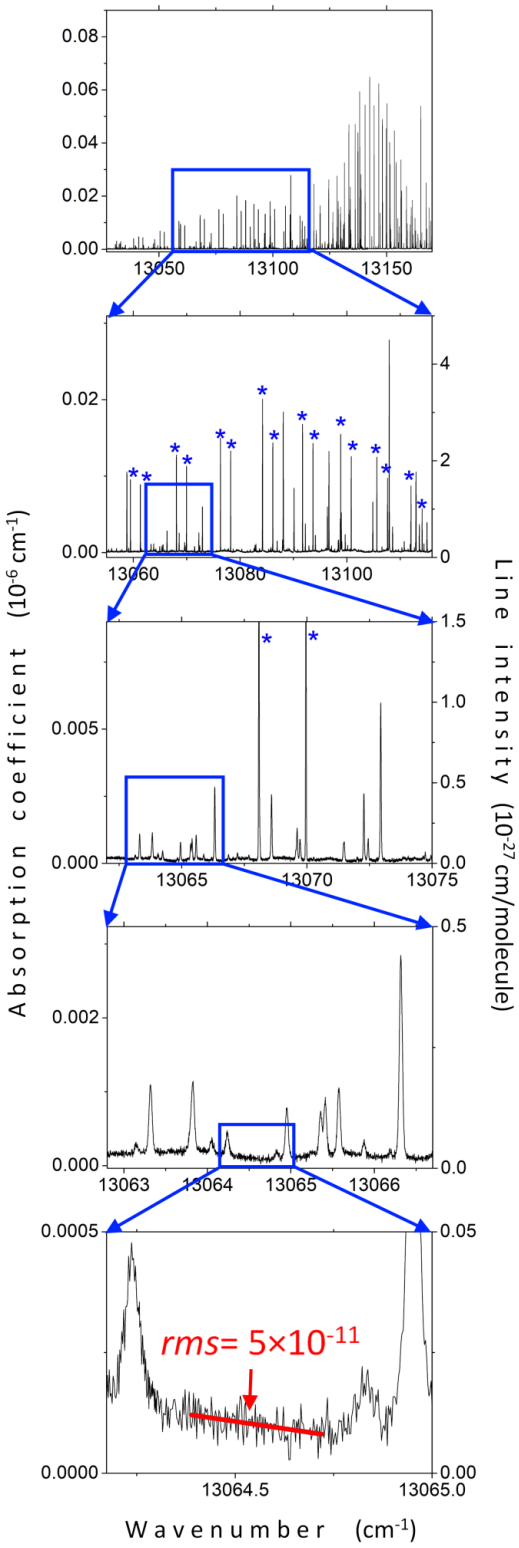

Fig. 3.
CRDS spectrum of water vapour at a pressure of about 19.0 Torr in the region of the A-band of oxygen. The strongest lines displayed on the upper panel are due to oxygen present in the cell with a relative concentration of a few 0.1%. The O_2 lines are marked with blue stars on the second and third panels. The right-hand intensity scale is adjusted to correspond approximately to the peak heights. The enlargements illustrate the dynamics achieved on the intensity scale and the noise equivalent absorption ($\alpha_{min} \approx 5\times10^{-11}$ cm^{-1}).

The pressure measured by a capacitance gauge (10 and 50 Torr Inficon CDG020D gauges having the accuracy of 0.5% of reading) and the ring down cell temperature were monitored during the recordings with 10 kΩ thermistor TDK B57861S.

The whole investigated region between 12967 and 13172 cm^{-1} was covered by four recordings at a pressure of about 9 Torr, each of them performed after renewal of the water vapor sample (the corresponding spectral intervals are 12969 - 13004, 13004.3 - 13026.3, 13025.5 - 13116.1 and 13115.9 - 13171.9 cm^{-1}). In addition, the central part of the region (13026.6 - 13141.7 cm^{-1}) was recorded at a pressure of 20 Torr. Let us mention that during the recordings, the ECDL source could not be tuned in a few narrow spectral intervals and the spectra show a ten of narrow (<1.3 cm^{-1}) spectral gaps below 13020 cm^{-1} (the corresponding spectral intervals are listed in the headings of the line list provided as Supplementary Material). The availability of two spectra over most of the studied spectral range allowed to reduce the number of missing lines. During the whole measurement campaign the temperature varied between 297 and 299 K.

The frequency calibration provided by the wavemeter was refined by shifting the whole spectrum in order to match accurate positions of $^{16}O_2$ lines provided in the HITRAN database [5]. After calibration, the *rms* value of the (meas. - HITRAN) position differences lines is less than 1×10^{-3} cm^{-1}, which is thus the estimated accuracy of the calibration of the frequency scale of the spectra.

Fig. 3 illustrates the sensitivity and high dynamical range on the intensity scale. The noise equivalent absorption evaluated as the root mean square (*rms)* of the baseline fluctuations is around 5×10^{-11} cm^{-1}. The spectrum is in fact dominated by lines of the A-band of oxygen. Due to a small leak, air is entering the CRDS cell. The air leak rate was evaluated from the oxygen absorption lines to be on the order of 8×10^{-4} Torr/hour. The recording times being limited to 15 hours at most, it leads to maximum partial pressures of air of about 10 mTorr which is negligible compared to the total pressure of 10 or 20 Torr.

The line centers and intensities were determined using an interactive least squares multi-lines fitting program written in LabVIEW. Most of the line profiles were assumed to be of Voigt type but for the strongest lines, the (obs. – calc.) residuals show the usual W-shape signature revealing the significance of collisional narrowing effects. The quadratic speed-dependent Nelkin Ghatak profile was adopted to fit the observed profile and derive the line position and integrated absorption coefficient. The HWHM of the Gaussian component was fixed to the theoretical value of the Doppler width of H_2O or O_2 (about 0.0189 cm^{-1} half-width at half-maximum for $H_2{}^{16}O$ at 296 K near 13000 cm^{-1}). Note that at the pressure of the recordings (10-20 Torr), the self- pressure broadening (in the 0.2-0.4 cm^{-1}/atm range [5]) is the main contribution to the line broadening. **Fig. 4** illustrates the quality of the spectrum fit near 13161 cm^{-1}.

The accuracy on the fitted line centers is estimated to be better than 3×10^{-3} cm^{-1} for unblended lines. This value includes the contribution of the unknown self-pressure shift of the line center.

According to the study of Grossman and Browell in the nearby region near 13800 cm^{-1} [21], the amplitude of the self-induced pressure shift coefficients was found to be less than 0.03 cm^{-1}/atm for most of the transitions leading to a maximum position shift less than 1×10^{-3} cm^{-1} at 20 Torr. The line center uncertainty will be confirmed below on the basis of combination difference relations.

After removal of the oxygen lines, the global line list between 12969 and 13172 cm^{-1} was obtained by merging the line lists obtained from the five recorded spectra. It includes a total of 692 lines. Next section is devoted to their rovibrational assignment.

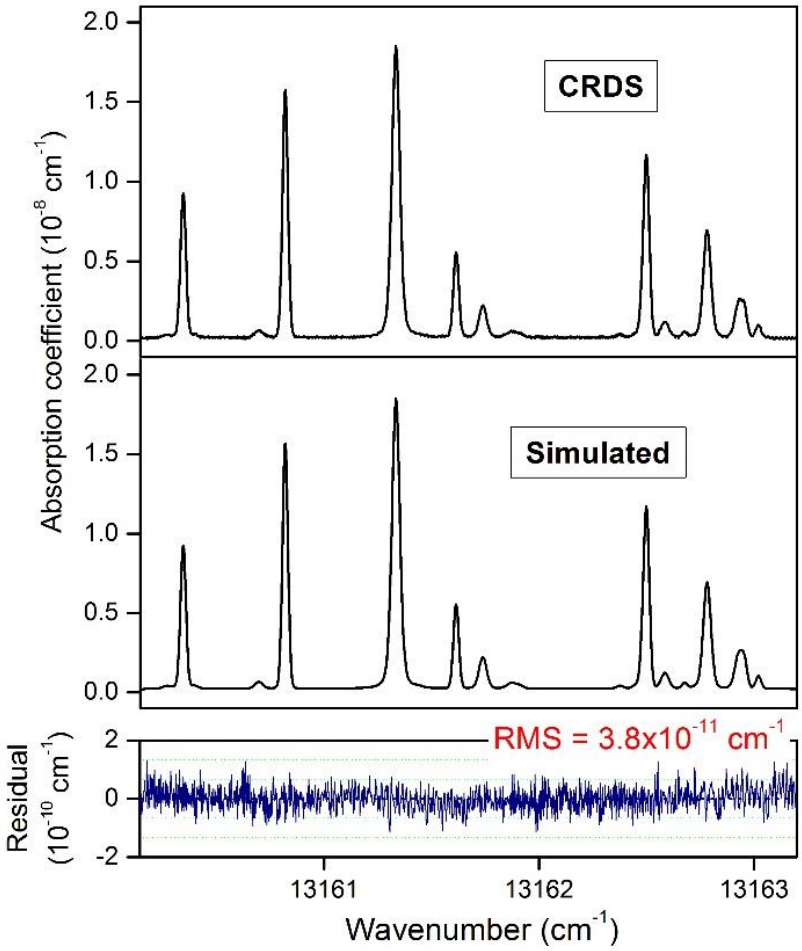

Fig. 4
Examples of the quality of spectra reproduction provided by the line profile fitting. The pressure of water vapor was about 19 Torr.

3. Rovibrational analysis

The rovibrational assignments were performed using the IUPAC empirical energy levels [22,23], the variational line list by Schwenke and Partridge (SP) [15-17] and the recent W2020 list [18]. 577 lines were assigned to 604 transitions of three water isotopologues ($H_2{}^{16}O$ – 539, $H_2{}^{18}O$ – 12 and $HD^{16}O$ – 53). In addition, 94 lines were assigned to oxygen ($^{16}O_2$ and $^{16}O^{18}O$) which is present in the sample with a relative concentration less than 0.1 % (see above). The rovibrational assignments are included in

the complete line list provided as Supplementary Material. Twenty-one lines with intensities smaller than 3.5×10^{-29} cm/molecule remain unassigned.

For the main isotopologue, $H_2{}^{16}O$, 519 lines were assigned to 539 transitions. For comparison, only about fifty $H_2{}^{16}O$ lines were previously assigned by ICLAS [7] in the region. The assigned transitions belong to 26 cold and two hot bands. Let us underline the difficulties related to the vibrational labelling. The SP line list [17] was taken as basis because it is the only available variational list that gives complete vibration-rotation labeling for all calculated transitions. The complexity of the vibrational labeling is due to the fact that at least 30 vibrational bands fall into the studied range. The rotational levels of most vibrational states are strongly mixed, so the vibrational labeling is often ambiguous. In general, the deviations of SP calculated line positions from the observed values have smooth vibration and rotation dependences (see, for example, Ref. [24]). These dependences *versus J* and K_a allow for assigning new energy levels when a sufficient series of deviations is available from already known levels. The problem of the studied spectral range is the reduced number of energy levels for the vibrational states of interest, especially those with a large excitation of the bending vibration: (080), (090), (150), (160), (250), etc. On the other hand, as noted in previous studies (see, for example, Ref. [19]), strong resonance perturbations can break the smooth dependences of deviations and some of the vibrational labeling remain ambiguous.

Overall, the assigned line positions allow us to determine 103 new upper energy levels for the main isotopologue. In addition, 135 upper energy levels were found to deviate by more than 5×10^{-3} cm^{-1} compared to the W2020 values [18] (see the discussion below). New and corrected term values are listed in **Table 1** and **2**, respectively.

The use of ground state combination differences (GSCD) is limited in the considered spectral region but upper state energies determined from two line positions provide a way to check our accuracy on the line positions. About 60 upper levels are involved in GSCD relations. The *rms* of the differences between the two independent determinations of the upper energy level is 4.2×10^{-3} cm^{-1} (2.5×10^{-3} cm^{-1} if we exclude the 15 levels for which one of the two lines is very weak or highly blended). These values are consistent with the claimed uncertainty of 3×10^{-3} cm^{-1} on the reported line positions.

The absorption spectrum of $H_2{}^{18}O$ in the region was studied by Leshchishina et al. [25] by ICLAS of a highly ^{18}O enriched sample. Twelve transitions of $H_2{}^{18}O$ in natural isotopic abundance, are identified in the present spectra. They belong to the $2\nu_1+4\nu_2$ and $\nu_1+4\nu_2+\nu_3$ bands. All but one are in good agreement with the results of Ref. [25]. The only significant difference concerns the $2\nu_1+4\nu_2$ $2_{02}-2_{11}$ transition observed at 13140.832 cm^{-1} in Ref. [25] which is not observed in the present work while its calculated intensity on the order of 10^{-29} cm/molecule [17,18] is above our detection threshold. As concerns the $HD^{16}O$ isotopologue, forty-eight lines of fifty-three transitions of the $2\nu_2+3\nu_3$ and $\nu_1+3\nu_3$ bands are assigned above 13049 cm^{-1}. The corresponding line positions are in good agreement with the results of Refs. [26-29]. The position differences $\delta\nu = |\nu^{Meas} - \nu^{Ref}|$ are larger than 0.01 cm^{-1} for only four

lines with maximum deviation of 0.017 cm^{-1} for the $2\nu_2+3\nu_3$ $6_{1\,5} - 7_{1\,6}$ transition at 13,165.4746 cm^{-1}. In addition, the lines of the $2\nu_2+3\nu_3$ $6_{1\,6} - 7_{07}$ and $\nu_1+3\nu_3$ $7_{43} - 8_{44}$ transitions are presently resolved (corresponding positions are 13,171.9145 and 13,171.9535 cm^{-1}, respectively) while a position value of 13,171.946 cm^{-1} was given in Refs. [26,27,29] for the unresolved doublet.

4. Comparison to literature line lists of $H_2{}^{16}O$

4.1 Experimental line lists

As mentioned above, due to the weakness of the water absorption lines in the region, previous experimental studies are very scarce. The only previous FTS observations in the considered region were reported by Tolchenov et al. [13] on the basis of spectra recorded at the Rutherford Appleton Laboratory (RAL) with long optical path lengths (up to 800.8 m) and a spectral resolution of 0.03 cm^{-1} [10,11]. The FTS list attached to Ref. [13] includes 72 lines in our region, twenty-four of them being assigned to $H_2{}^{16}O$ transitions (see **Fig. 5**). The comparison to the CRDS observations indicates that 15 of these 24 lines assigned to water are in fact A-band oxygen lines, as clearly apparent on **Fig. 5** (upper panel). This assignment error was already mentioned in Ref. [7]. Note that half of the O_2 lines erroneously assigned to water in [13] were kept in the transition database used to determine the IUPAC-TG [23] and W2020 [18] energy levels. Only five of the FTS assigned lines are confirmed by the present more sensitive CRDS measurements. Five additional water lines could be identified among the unassigned FTS lines of Ref. [13] but, overall, most of the reported lines are in fact artifacts or O_2 lines.

The ICLAS study allowed for the assignment of forty-nine $H_2{}^{16}O$ transitions in the region [7] with intensities above 10^{-27} cm/molecule, two orders of magnitude above the present CRDS detectivity threshold **(Fig. 5**, middle panel). All but one ICLAS lines are confirmed by the present CRDS recordings. The line at 13151.8818 cm^{-1} reported with no assignment in Ref. [7] is also confirmed and corresponds to the $2\nu_1+4\nu_2$ $3_{3\,0} - 4_{4\,1}$ transition. The *rms* value of the differences ($\delta\nu = \nu^{CRDS} - \nu^{ICLAS}$) is 0.0075 cm^{-1} with maximum deviation of about 0.02 cm^{-1} for the three weakest lines. This is consistent with the uncertainty of 0.004 cm^{-1} on the ICLAS line positions [7] combined to the present 0.003 cm^{-1} estimated uncertainty on the CRDS values.

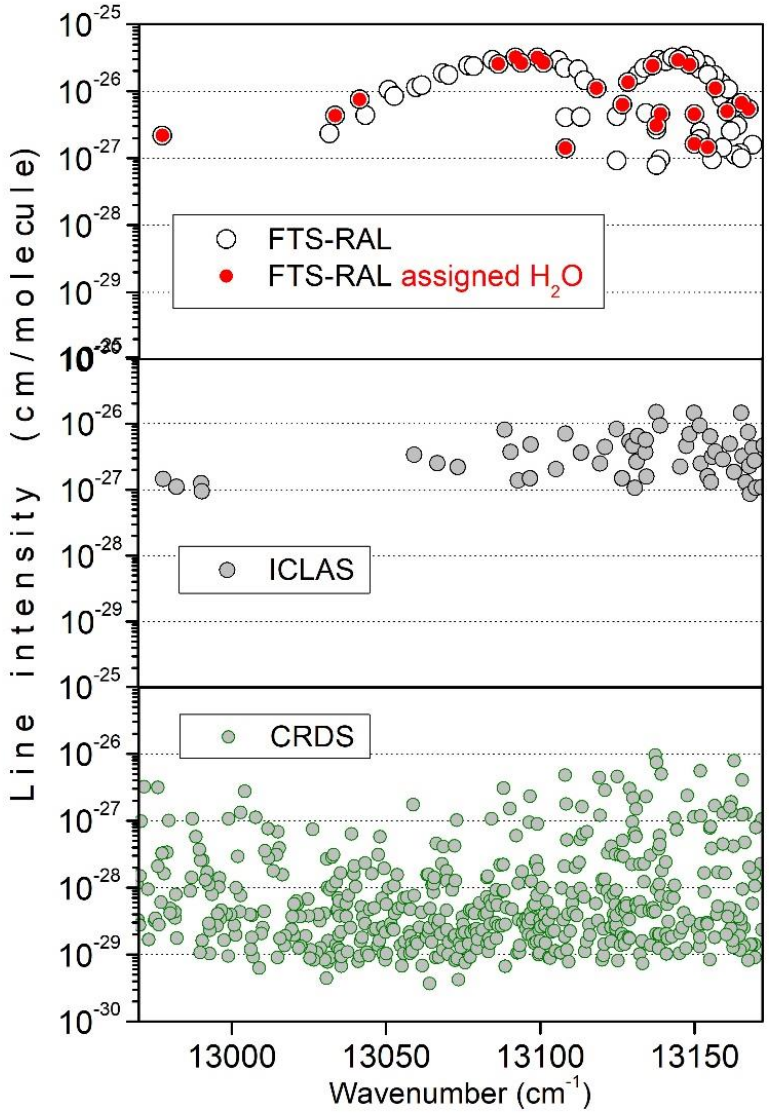

Fig. 5

Overview comparison of the experimental line list of $H_2{}^{16}O$ in the region of the A band of oxygen obtained by FTS [13], ICLAS [7] and in the present work. In the case of the FTS dataset (upper panel), the lines assigned to water are highlighted (full red circles). In fact, most of FTS lines belong to the oxygen A band.

4.2 SP, W2020 and HITRAN2016 line lists

In the following, the recorded CRDS spectra and corresponding experimental list are used for comparison to the variational list by Schwenke and Partridge [15-17], to the very recent W2020 line list of $H_2{}^{16}O$ [18] and to the HITRAN2016 list [5]. The series of examples displayed on **Figs. 6** and **7** illustrate some position and intensity discrepancies between the observations and the W2020 and HITRAN2016 lists. The HITRAN2016 line positions in the region rely mostly on the IUPAC-TG line positions [23]. As intensity measurements are mostly absent in the region, the HITRAN2016 list reproduces BT2 line intensities computed variationally using an *ab initio* dipole moment surface [30].

As concerns the W2020 line positions, most of them were empirically corrected using an updated of the IUPAC-TG energy levels [7]. Otherwise, the W2020 positions are variational values. On **Figs. 6** and **7**, the W2020 variational position values are displayed without error bar while the W2020 uncertainty is displayed in the cases of empirical values. Note that the right-hand intensity scale has been adjusted to correspond approximately to the peak heights

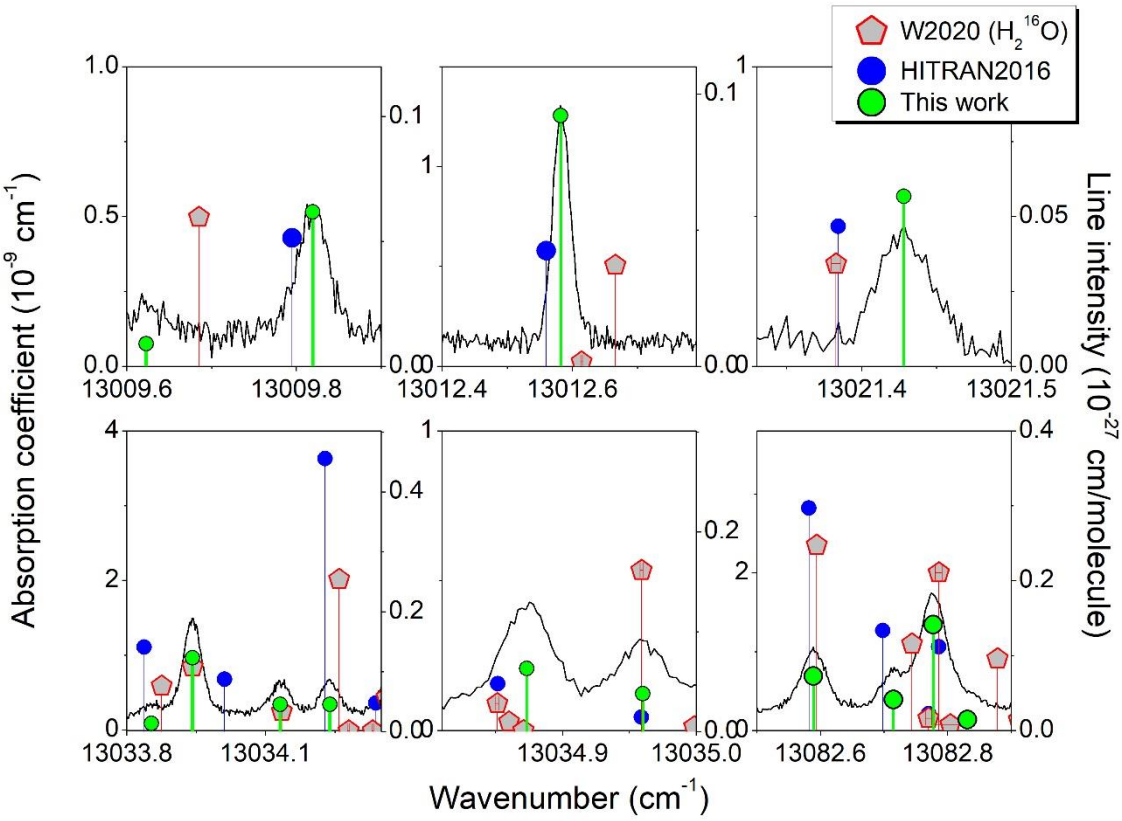

Fig. 6

Examples of comparison of the CRDS spectrum of water vapor and corresponding line list (green circles) to the W2020 line list of $H_2{}^{16}O$ [18] (grey pentagons) and the HITRAN2016 lists of natural water (blue circles). In the cases of line positions based on empirically determined energy levels, the W2020 error bars are displayed. The right-hand intensity scale is adjusted to correspond approximately to the peak heights

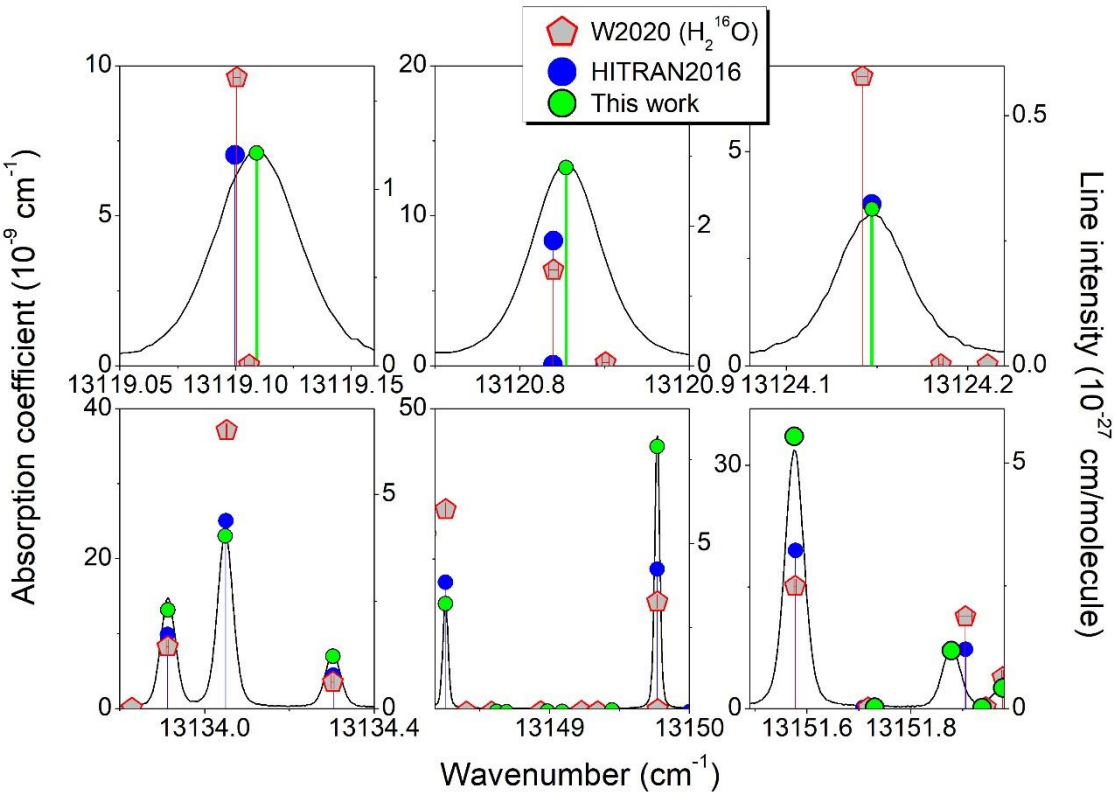

Fig. 7
Examples of comparison of the CRDS spectrum of water vapor to the W2020 line list of $H_2^{16}O$ [18] (grey pentagons) and the HITRAN2016 lists of natural water (blue circles). See caption of Fig. 6.

The first step for a systematic comparison between the SP and W2020 line lists and our $H_2^{16}O$ experimental list was to identify the corresponding transitions in the different lists. Identical lower state and upper J values, close values of the positions and intensities (within 0.3 cm^{-1} and 20-30 %, respectively) and the rovibrational assignment (when available) were used as criteria. A significant number of the W2020 transitions are provided without vibrational labeling of the upper level and without K_a and K_c values (only the J value is given). In addition, part of the SP assignments is ambiguous due to numerous resonances. In the global list provided as Supplementary Material, for each observed transition, the corresponding SP and W2020 position and intensity values are given. Note that the vibrational labeling of more than one hundred-twenty W2020 transitions were modified or completed. The list includes the original W2020 assignments when they have been changed.

Line positions

Fig. 8 shows the overview of the deviations of the W2020 and SP position values from the corresponding CRDS values. SP position values were not empirically corrected and are thus, all, variational values. In the case of the W2020 list, the positions relying on empirical energy levels and those with variational origin are distinguished (blue full squares and red open circles, respectively). The *rms* value of the differences is 0.182 cm^{-1} for the SP list (536 positions) while for the W2020 list, *rms*

values of 0.032 and 0.151 cm^{-1} are obtained for 419 empirical and 111 variational positions, respectively. Note that the large $\delta\nu$ = -1.075 cm^{-1} position difference for the $7\nu_2+\nu_3$ $11_{1\,11} - 12_{5\,8}$ transition was not taken into account in the calculation of the W2020 *rms* and is not shown on **Fig. 8**. The W2020 error bar attached to this position is 0.00176 cm^{-1}, more than 600 times larger than the position difference ($\delta\nu = \nu^{CRDS} - \nu^{W2020}$). This is an extreme example of underestimation of the W2020 position uncertainties.

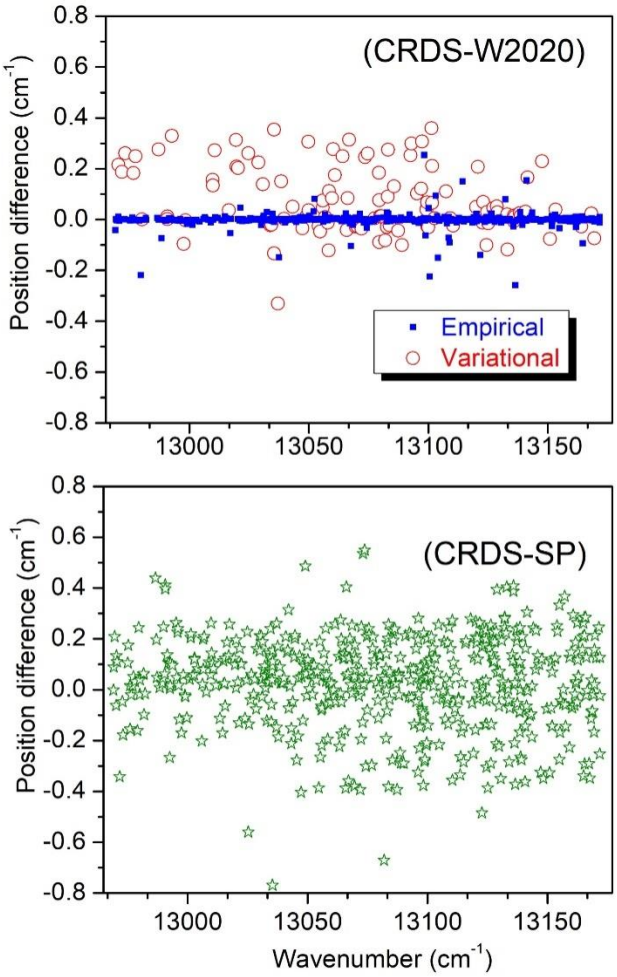

Fig. 8
Overview of the position differences between the present CRDS values and the W2020 [18] and SP [17] position values (upper and lower panels, respectively). The W2020 differences corresponding to empirical and variational values have been distinguished (blue full squares and red open circles, respectively).

We have included in the global list provided as Supplementary Material, the ratio $R=\frac{|Measured-W2020|}{UncW2020}$ corresponding to the absolute deviation of the W2020 position from the CRDS value. Among the 420 positions relying on W2020 empirical energy levels, 245 have a deviation exceeding the claimed W2020 position uncertainty ($R > 1$). Among these, 183 deviate by more than the estimated uncertainty on the CRDS line positions (3×10^{-3} cm^{-1}). Some significant deviations are illustrated in **Figs. 6** and **7**. Let us recall that only about 50 line positions were reliably reported from

absorption spectrum in the region [7]. The 420 W2020 empirical positions rely thus not only on the ICLAS measurements but also on energy levels retrieved from measurements performed in different spectral regions, in particular less accurate emission spectra [18]. The agreement between the W2020 and CRDS position values is not satisfactory and reveals deficiencies of the xMARVEL procedure used to derive the W2020 energy levels and evaluate the uncertainty of the used data sources [18]. We note for instance that the W2020 list in the region includes some lines with position accuracy as good as 2×10^{-5} cm^{-1} while the ICLAS positions have a claimed accuracy of 4×10^{-3} cm^{-1} [7] i. e. two hundred times larger.

More problematic is the fact that the oxygen lines erroneously assigned as water transitions in Ref. [13] are included in the W2020 transition database and have strong impact on some of the W2020 energy values:

(i) the W2020 energy values of the (061) $10_{2\,9}$ and (061) $7_{3\,4}$ levels of $H_2{}^{16}O$ rely on the 13041.127659 and 13118.04496 cm^{-1} FTS line positions [13], assigned as (061) $10_{2\,9}$ – (000) $9_{2\,8}$ and (061) $7_{3\,4}$ – (000) $6_{3\,3}$, respectively, while these lines are O_2 lines (at 13041.123638 and 13118.044663 cm^{-1}, respectively, according to HITRAN2016 [5]). The W2020 uncertainties claimed for the (061) $10_{2\,9}$ and (061) $7_{3\,4}$ levels are about 2×10^{-3} cm^{-1}.

(ii) the W2020 energy value of the (061) $6_{3\,3}$ level uses the FTS line position at 13100.823102 cm^{-1} assigned to the (061) $6_{3\,3}$ – (000) $5_{3\,2}$ while it corresponds to the O_2 line at 13100.821753 cm^{-1} [5]. Our CRDS position for the same transition (13100.59815 cm^{-1}) leads to a correction of the energy value of 0.225 cm^{-1}, more than 130 times the W2020 uncertainty attached to the considered level (1.71×10^{-3} cm^{-1}) [18].

More details about the inclusion of the O_2 line positions of Ref. [13] in the W2020 transition database and its impact on some W2020 energy levels of $H_2{}^{16}O$ is provided as a Supplementary Material.

We have included in the last column of **Table 2**, the ratio $R=\frac{|Meas.-W2020|}{UncW2020}$ corresponding to the absolute deviation of the W2020 upper energy value from the experimental value derived from the present CRDS measurements. For 115 of the 135 levels of **Table 2**, the deviation exceeds the W2020 stated accuracy ($R > 1$).

Line intensities

A number of spectral intervals showing important disagreement between the experimental spectrum and the HITRAN2016 and W2020 line lists are displayed in **Figs. 6 and 7**. Let us recall that both HITRAN2016 and W2020 intensities have variational origin, from BT2 [30] and PoKaZaTeL [31], respectively. This situation reflects the difficulties to compute the intensities of the transitions in the region. Surprisingly, in a number of cases, the BT2 intensities included in HITRAN2016 agree better with the observations than the PoKaZaTeL intensities of the W2020 list. The large differences between the SP, BT2 and PoKaZaTeL intensities show the high sensitivity of the computed intensities to small changes in the potential energy or dipole moment surfaces in the considered region. This is probably

related to the high excitation of the involved upper levels and to the fact that many of them involve a high bending excitation.

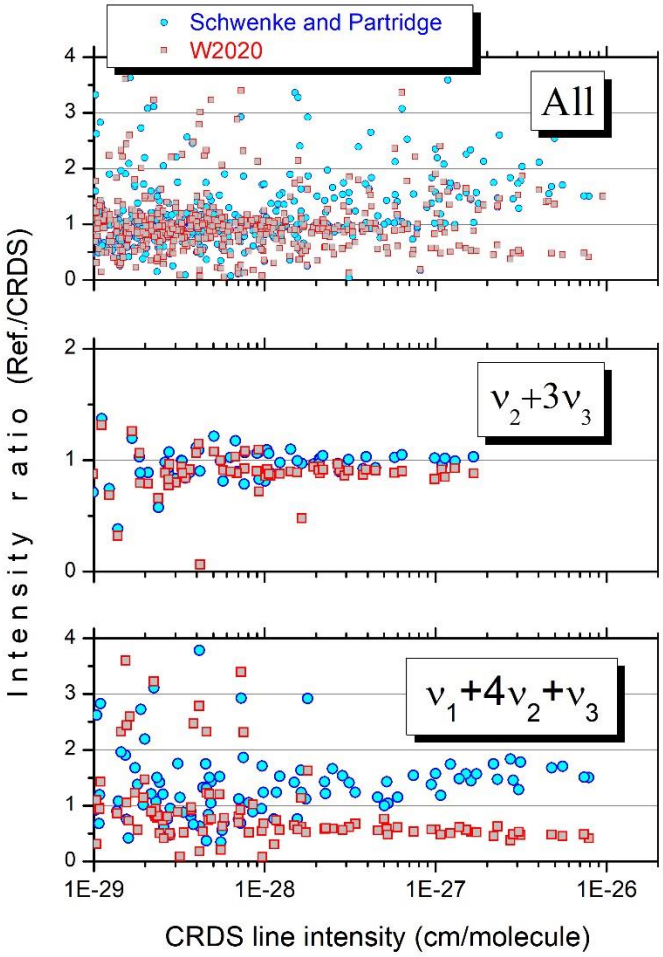

Fig. 9

Overview of the intensity ratios of SP [17] and W2020 [18] variational values to the CRDS values (blue circles and red squares, respectively) *versus* the CRDS intensity values. On the upper panel, all the ratios of the $H_2{}^{16}O$ transitions measured in the 12969-13172 cm^{-1} are displayed. The two lower panels are limited to the ratios relative to the $\nu_2+3\nu_3$ and $\nu_1+4\nu_2+\nu_3$ bands.

The ratios of the SP and W2020 variational values to the CRDS intensity values are displayed in **Fig. 9** (upper panel). A large dispersion is noted for both SP and W2020 ratios, although more pronounced in the case of SP values. The ratios corresponding to the line intensities of the $\nu_2+3\nu_3$ and $\nu_1+4\nu_2+\nu_3$ bands have been separated on the middle and lower panels of the figure. In the case of the $\nu_2+3\nu_3$ band, the SP and PoKaZaTeL intensities are close and agree with the experimental values, although a systematic shift of about +3% and -11 % is noted for SP and PoKaZaTeL, respectively. The observed dispersion on the ratios provides a validation of the claimed uncertainty of the experimental intensities of about 5 % for most of the lines. In the case of $\nu_1+4\nu_2+\nu_3$ band, the experimental intensities

are also intermediate between the two calculations but the difference is much larger, PoKaZaTeL intensities of the W2020 list being about twice smaller than measured while SP values are on average 50 % larger than measured. The fact that both calculations show a good agreement with measurements for the $\nu_2+3\nu_3$ band and a worse agreement for the $\nu_1+4\nu_2+\nu_3$ band, may indicate that the latter is more sensitive to small changes of the potential energy or dipole moment surfaces.

5. Recommended line list and concluding remarks

While variational intensities have been validated in some lower energy regions, in the considered region, the comparison of the variational line intensities (SP [17], BT2 [30] in HITRAN, and PoKaZaTeL [31] in W2020) shows a large dispersion and significant deviations from the measured values. For example, SP list contains about 30 relatively strong transitions (up to 2×10^{-27} cm/molecule) of bands with a large bending excitation ($9\nu_2$, $8\nu_2$, $\nu_1+6\nu_2$, $6\nu_2+\nu_3$) that are not observed in the spectrum in spite of a detectivity threshold on the order of 10^{-29} cm/molecule. The SP intensity of these lines are this believed to be strongly overestimated. On the basis of the above comparisons, it appears that line parameters of water vapor transitions to be recommended in the region of the oxygen A-band are thus experimental values both for line positons and for line intensities.

In order to generate a recommended line list for the region, the CRDS line list provided as Supplementary Material was cleaned from unassigned and oxygen lines and completed in the narrow spectral intervals which were not covered by the recordings. The intensity cut off of the recommended list provided as a separate Supplementary Material is fixed to 1×10^{-29} cm/molecule. Overall 89 transitions of the W2020 list predicted to be located in spectral gaps of the recordings or missing in the experimental list because they are obscured by much stronger lines, were incorporated in the recommend list. The total line list includes 693 transitions of $H_2{}^{16}O$, $H_2{}^{18}O$ and $HD^{16}O$.

In summary, the knowledge of the very weak absorption spectrum of water vapor has been significantly improved in the region of the oxygen A-band near 760 nm. The reported results were obtained on the basis of high sensitivity CRDS recordings which improved by two orders of magnitude the sensitivity of previous ICLAS observations [7]. These spectra are the first spectra recorded with a new CRDS spectrometer developed at the Institute of Atmospheric Optics (Tomsk) following the optical arrangement and data acquisition procedure of the CRDS spectrometers developed in Grenoble [19,20].

Overall, the negligible impact of the interfering lines of atmospheric water vapor on the air-mass retrieval based on the A-band of oxygen is confirmed. Nevertheless, the recorded spectra provide valuable validation tests for the different line lists covering this region. Significant differences are noted both for positions and intensities compared to the SP, HITRAN2016 and W2020 lists (see **Figs. 6 and 7**). The deficiencies in terms of line positions are due to the lack of previous measurements. Nevertheless, in the W2020 line list [18] most of the line positions rely on empirically upper energy values and are reported with small error bars. Among the 420 positions relying on W2020 empirical

energy levels, 183 deviate by more than the estimated uncertainty on the CRDS line positions (3×10^{-3} cm^{-1}). Deviations exceeding the W2020 error bars by a factor of ten or more are noted, indicating that the W2020 error bars are largely underestimated in the region.

Acknowledgements
The support of the CNRS (France) in the frame of International Research Project SAMIA is acknowledged. CRDS measurements and spectrum analysis were performed at IAO-Tomsk and funded by RFBR project 20-32-70054.

References

[1] Goody RM, Yung YL. Atmospheric Radiation. Theoretical Basis. 2nd edition. New York: Oxford University Press; 1990. doi: 10.1093/oso/9780195051346.001.0001.

[2] Washenfelder RA, Toon GC, Blavier JF, Yang Z, Allen NT, Wennberg PO, et al. Carbon dioxide column abundances at the Wisconsin Tall Tower site. J Geophys Res Atmos 2006;111. https://doi.org/10.1029/2006JD007154.

[3] Long DA, Havey DK, Okumura M, Miller CE, Hodges JT. O_2 A-band line parameters to support atmospheric remote sensing. J Quant Spectrosc Radiat Transf 2010;111:2021–36. https://doi.org/10.1016/j.jqsrt.2010.05.011.

[4] Wunch D, Toon GC, Blavier J-FL, Washenfelder RA, Notholt J, Connor BJ, et al. The total carbon column observing network. Philos Trans R Soc London A Math Phys Eng Sci 2011;369:2087–112. https://doi.org/10.1098/rsta.2010.0240.

[5] Gordon IE, Rothman LS, Hill C, Kochanov RV, Tan Y, Bernath PF, et al. The HITRAN2016 molecular spectroscopic database. J Quant Spectrosc Radiat Transf 2017;203:3–69. https://doi.org/10.1016/j.jqsrt.2017.06.038.

[6] Jacquinet-Husson N, Armante R, Scott NA, Chédin A, Crépeau L, Boutammine C, et al. The 2015 edition of the GEISA spectroscopic database. J Mol Spectrosc 2016;327:31–72. https://doi.org/10.1016/j.jms.2016.06.007.

[7] Campargue A, Mikhailenko S, Liu AW. ICLAS of water in the 770 nm transparency window (12 746 − 13 558 cm^{-1}). Comparison with current experimental and calculated databases. J Quant Spectrosc Radiat Transf 2008;109:2832–45. https://doi.org/10.1016/j.jqsrt.2008.07.003.

[8] Coheur PF, Fally S, Carleer M, Clerbaux C, Colin R, Jenouvrier A, et al. New water vapor line parameters in the 26000 − 13000 cm^{-1} region. J Quant Spectrosc Radiat Transf 2002;74:493–510. https://doi.org/10.1016/S0022-4073(01)00269-2.

[9] Mérienne MF, Jenouvrier A, Hermans C, Vandaele AC, Carleer M, Clerbaux C, et al. Water vapor line parameters in the 13 000 9250 cm^{-1} region. J Quant Spectrosc Radiat Transf 2003;82:99–117. https://doi.org/10.1016/S0022-4073(03)00148-1.

[10] Schermaul R, Learner RCM, Newnham DA, Ballard J, Zobov NF, Belmiloud D, et al. The water vapor spectrum in the region 8600-15 000 cm^{-1}: Experimental and theoretical studies for a new spectral line database:I: Laboratory measurements J Mol Spectrosc, 208 (2001), pp. 32-42. doi.org/10.1006/jmsp.2001.8373

[11] Schermaul R, Learner RCM, Newnham DA, Ballard J, Zobov NF, Belmiloud D, et al. The water vapor spectrum in the region 8600 − 15 000 cm^{-1}: Experimental and theoretical studies for a new spectral line database: II. Linelist construction. J Mol Spectrosc 2001;208:43–50. https://doi.org/10.1006/jmsp.2001.8374.

[12] Tolchenov RN, Naumenko O, Zobov NF, Shirin SV, Polyansky OL, Tennyson J, et al. Water vapour line assignments in the 9250 − 26 000 cm^{-1} frequency range. J Mol Spectrosc 2005;233:68–76. https://doi.org/10.1016/j.jms.2005.05.015.

[13] Tolchenov RN, Tennyson J, Brault JW, Canas AAD, Schermaul R. Weak line water vapor spectrum in the 11 787 − 13 554 cm^{-1} region. J Mol Spectrosc 2002;215:269–74. https://doi.org/10.1006/jmsp.2002.8653.

[14] Campargue A, Stoeckel F, Chenevier M. High sensitive intracavity laser spectroscopy: Application to the study of overtone transitions in the visible range. Spectrochim Acta Rev 1990;13:69-88.

[15] Partridge H, Schwenke DW. The determination of an accurate isotope dependent potential energy surface for water from extensive ab initio calculations and experimental data. J Chem Phys 1997;106:4618–39. https://doi.org/10.1063/1.473987.

[16] Schwenke DW, Partridge H. Convergence testing of the analytic representation of an *ab initio* dipole moment function for water: Improved fitting yields improved intensities. J Chem Phys 2000;113:6592–7. https://doi.org/10.1063/1.1311392.

[17] Tashkun SA. Institute of Atmospheric Optics SB RAS. 2007. http://spectra.iao.ru/molecules/simlaunch?mol=1

[18] Furtenbacher T, Tóbiás R, Tennyson J, Polyansky OL, Kyuberis AA, Ovsyannikov RI, et al. The W2020 Database of Validated Rovibrational Experimental Transitions and Empirical Energy Levels of Water Isotopologues. II. $H_2{}^{17}O$ and $H_2{}^{18}O$ with an update to $H_2{}^{16}O$. J Phys Chem Ref Data 2020;49:43103. https://doi.org/10.1063/5.0030680.

[19] Macko P, Romanini D, Mikhailenko SN, Naumenko OV, Kassi S, Jenouvrier A, et al. High sensitivity CW-cavity ring down spectroscopy of water in the region of the 1.5 μm atmospheric window. J Mol Spectrosc 2004;227:90–108. https://doi.org/10.1016/j.jms.2004.05.020.

[20] Kassi S, Campargue A. Cavity ring down spectroscopy with 5×10^{-13} cm^{-1} sensitivity. J Chem Phys 2012;137. https://doi.org/10.1063/1.4769974.

[21] Grossmann BE, Browell EV. Spectroscopy of water vaporin the 720-m wavelength region: line strengths, self-induced pressure broadenings and shifts, and temperature dependence of line widths and shifts. J Mol Spectrosc 1989;136(2):264–94. doi:10.1016/0022-2852(89)90336-6.

[22] Tennyson J, Bernath PF, Brown LR, Campargue A, Császár AG, Daumont L, et al. IUPAC critical evaluation of the rotational-vibrational spectra of water vapor. Part II. Energy levels and transition wavenumbers for $HD^{16}O$, $HD^{17}O$, and $HD^{18}O$. J Quant Spectrosc Radiat Transf 2010;111:2160–84. https://doi.org/10.1016/j.jqsrt.2010.06.012.

[23] Tennyson J, Bernath PF, Brown LR, Campargue A, Császár AG, Daumont L, et al. IUPAC critical evaluation of the rotational-vibrational spectra of water vapor, Part III: Energy levels and transition wavenumbers for $H_2{}^{16}O$. J Quant Spectrosc Radiat Transf 2013;117:29–58. https://doi.org/10.1016/j.jqsrt.2012.10.002.

[24] Campargue A, Vasilenko I, Naumenko O. Intracavity laser absorption spectroscopy of HDO between 11 645 and 12 330 cm^{-1}. J Mol Spectrosc 2005;234:216–27. https://doi.org/10.1016/j.jms.2005.09.007.

[25] Leshchishina OM, Naumenko OV, Campargue A. High sensitivity ICLAS of $H_2{}^{18}O$ in the 12,580 - 13,550cm-1 transparency window. J Quant Spectrosc Radiat Transf 2011;112:913–24. https://doi.org/10.1016/j.jqsrt.2010.11.012.

[26] Naumenko O, Bertseva E, Campargue A, Schwenke DW. Experimental and *ab initio* studies of the HDO absorption spectrum in the 13 165 − 13 500 cm^{-1} spectral region. J Mol Spectrosc 2000;201:297–309. https://doi.org/10.1006/jmsp.2000.8087.

[27] Voronin BA, Naumenko O V., Carleer M, Coheur PF, Fally S, Jenouvrier A, et al. HDO absorption spectrum above 11 500 cm^{-1}: Assignment and dynamics. J Mol Spectrosc 2007;244:87–101.

https://doi.org/10.1016/j.jms.2007.03.008.

[28] Naumenko OV, Voronin BA, Mazzotti F, Tennyson J, Campargue A. Intracavity laser absorption spectroscopy of HDO between 12 145 and 13 160 cm^{-1}. J Mol Spectrosc 2008;248:122–33. https://doi.org/10.1016/j.jms.2007.12.005.

[29] Naumenko OV, Béguier S, Leshchishina OM, Campargue A. ICLAS of HDO between 13,020 and 14,115 cm^{-1}. J Quant Spectrosc Radiat Transf 2010;111:36–44. https://doi.org/10.1016/j.jqsrt.2009.06.016.

[30] Barber RJ, Tennyson J, Harris GJ, Tolchenov RN. A high-accuracy computed water line list. Mon Not R Astron Soc 2006;368:1087. https://doi.org/10.1111/j.1365-2966.2006.10184.x.

[31] Polyansky OL, Kyuberis AA, Zobov NF, Tennyson J, Yurchenko SN, Lodi L. ExoMol molecular line lists XXX: A complete high-accuracy line list for water. Mon Not R Astron Soc 2018;480:1–12. https://doi.org/10.1093/mnras/sty1877.

Table 1
Energy levels of $H_2{}^{16}O$ newly determined from the analysis of the CRDS spectra of water vapor between 12969 and 13172 cm^{-1}

$V_1V_2V_3$	J	Ka	Kc	Energy (cm^{-1})
013	9	9	1	14689.97333
013	10	8	2	14728.36838
013	11	7	5	14804.30313
013	11	7	4	14804.20305
013	12	4	9	14618.09563
013	12	5	8	14761.93765
013	12	6	7	14917.67635
013	12	6	6	14923.63391
013	12	7	5	15082.18121
013	13	5	9	15063.88046
013	13	5	8	15141.21927
013	13	6	8	15222.35057
013	14	4	10	15372.00024
032	11	8	4	14798.17399
032	11	8	3	14798.04510
042	7	2	6	14218.35022
061	4	3	1	13342.26938
061	5	2	3	13220.30757
061	5	3	3	13462.83380
061	5	3	2	13463.61503
061	7	2	5	13549.24158
061	7	4	4	14064.39676
061	7	4	3	14060.53386
061	7	5	2	14383.14225
061	8	3	6	13959.82103
061	8	4	4	14250.90589
061	8	5	4	14576.52473
061	8	5	3	14576.75448
061	10	1	9	14059.16480
061	12	6	6	15904.06833
080	5	5	1	13772.29639
080	9	4	5	14043.18505
080	9	6	3	15120.53258
090	2	1	2	13093.35475
090	2	1	1	13117.41919
090	3	1	3	13153.80334
090	3	1	2	13202.63926
112	12	2	10	14304.54597
112	13	3	11	14568.33807
112	13	6	8	15092.89625
112	14	2	12	14856.41387
112	14	4	11	15061.70226
112	14	5	10	15239.52041
131	10	7	4	14226.05053
131	12	7	5	14783.42555
131	13	6	8	14747.87320
141	9	1	8	14375.98552
141	11	3	8	15166.74934
141	12	1	11	15080.74205
141	13	2	12	15337.53548
150	13	7	6	14751.24824
160	3	3	1	13170.01676
160	3	3	0	13169.14066
160	4	3	2	13266.18841
160	4	3	1	13264.22731
160	5	3	3	13386.05203
160	5	3	2	13382.95148
160	5	5	1	14035.77022
160	5	5	0	14035.76972
160	6	3	4	13529.22543
160	6	3	3	13525.35866
160	6	5	2	14180.86051
160	6	5	1	14180.86101
160	7	2	5	13444.76035
160	7	3	4	13691.54001
160	7	4	4	14011.51268
160	7	5	3	14349.24163
160	8	2	6	13644.83033
160	8	4	5	14202.08645
160	8	4	4	14188.50739
160	8	5	4	14540.51450
160	9	2	7	13868.69786
160	10	3	8	14343.53315
160	10	4	7	14649.20039
160	12	6	7	16069.44166
211	9	9	1	14285.86204
221	12	5	7	16020.48604
230	12	8	5	14784.92648
240	9	2	8	14336.25352
240	10	1	9	14545.41478
240	10	3	8	14774.27349
240	10	5	5	15237.87526
240	11	1	10	14779.66312
240	11	2	10	14774.54050
240	11	3	9	15018.63616
240	12	2	11	15022.14767
250	1	1	0	14673.26365
250	2	1	2	14705.94254
250	3	0	3	14712.50702
250	3	1	2	14803.90485
250	3	2	1	14923.31216
250	4	1	4	14842.25704
250	5	0	5	14903.49283
250	6	1	6	15057.02337
250	7	0	7	15165.44647
250	8	0	8	15321.74707
301	11	5	7	15632.51276
320	12	3	10	15554.05794
400	10	9	2	16028.65360
400	10	9	1	16028.65360
400	11	7	5	15913.11523
400	12	0	12	15276.89660
400	12	7	6	16187.97226

Table 2
Energy levels of $H_2{}^{16}O$ showing differences larger than 5×10^{-3} cm^{-1} with the corresponding W2020 empirical values [18].

$(V_1V_2V_3)$	J	Ka	Kc	Energy level (cm^{-1})			UncW2020	R [a]
				This Work	W2020	Difference (TW-W2020)		
004	6	1	6	14956.24512	14956.25658	-0.01146	0.00193	5.9
013	7	6	1	13733.84058	13733.83314	0.00744	0.00160	4.7
013	7	7	0	13900.46984	13900.46376	0.00608	0.01362	0.4
013	7	7	1	13900.46911	13900.46372	0.00539	0.01362	0.4
013	8	7	1	14090.68087	14090.67483	0.00604	0.00132	4.6
013	8	8	0	14275.34322	14275.33675	0.00647	0.00101	6.4
013	9	5	4	13990.71338	13990.72967	-0.01629	0.00336	4.8
013	9	7	2	14304.64348	14304.63553	0.00795	0.00288	2.8
013	9	8	2	14490.32923	14490.32410	0.00513	0.00110	4.7
013	10	5	5	14231.01710	14231.02431	-0.00721	0.00181	4.0
013	10	5	6	14222.79546	14222.78807	0.00739	0.00756	1.0
013	10	7	3	14542.24895	14542.25573	-0.00678	0.00200	3.4
013	11	3	8	14333.19524	14333.20776	-0.01252	0.00142	8.8
013	12	5	7	14822.18592	14822.19792	-0.01200	0.00400	3.0
013	13	4	10	14911.19100	14911.19821	-0.00721	0.00200	3.6
023	8	2	6	15044.99851	15045.00390	-0.00539	0.00126	4.3
023	11	2	10	15545.65892	15545.67215	-0.01323	0.00479	2.8
032	9	8	2	14328.99997	14329.01223	-0.01226	0.00303	4.0
042	3	1	2	13645.64140	13645.64674	-0.00534	0.00253	2.1
042	5	3	2	14076.13846	14076.12414	0.01432	0.00146	9.8
042	6	3	4	14215.89351	14215.90248	-0.00897	0.00123	7.3
042	8	2	7	14391.52821	14391.51880	0.00941	0.01938	0.5
061	4	3	2	13342.07008	13342.05112	0.01896	0.01004	1.9
061	6	2	4	13371.63639	13371.62917	0.00722	0.00603	1.2
061	6	3	3	13609.41015	13609.63587	-0.22572	0.00171	132.0
061	6	3	4	13607.09861	13607.00613	0.09248	0.00250	37.0
061	6	5	1	14212.95742	14212.93984	0.01758	0.01229	1.4
061	7	3	5	13772.79815	13772.80650	-0.00835	0.00156	5.4
061	7	5	3	14383.03636	14383.04702	-0.01066	0.00145	7.4
061	9	2	8	13896.39710	13896.38854	0.00856	0.01452	0.6
061	9	3	7	14184.27475	14184.26890	0.00585	0.01004	0.6
071	11	1	11	15302.00046	15303.07660	-1.07614	0.00723	148.8
080	5	5	0	13772.25023	13772.28061	-0.03038	0.00400	7.6
090	4	1	4	13235.01991	13234.76685	0.25306	0.03731	6.8
090	6	1	6	13461.90019	13462.15970	-0.25951	0.02092	12.4
103	10	2	8	15660.75418	15660.72549	0.02869	0.00198	14.5
112	12	3	10	14297.70993	14297.71585	-0.00592	0.00629	0.9
112	13	2	11	14562.14736	14562.15555	-0.00819	0.00424	1.9
112	14	3	12	14858.71653	14858.68634	0.03019	0.01887	1.6
122	10	2	9	15163.47957	15163.46847	0.01110	0.01151	1.0
122	10	5	6	15657.87321	15657.90133	-0.02812	0.00300	9.4
131	9	7	3	13985.78984	13986.01019	-0.22035	0.00250	88.1
141	1	0	1	13279.36328	13279.35111	0.01217	0.02822	0.4
141	2	0	2	13324.80857	13324.81477	-0.00620	0.00218	2.8
141	4	1	4	13487.95863	13487.96585	-0.00722	0.00496	1.5
141	5	0	5	13576.47472	13576.46858	0.00614	0.01337	0.5
141	6	1	5	13825.04135	13825.03407	0.00728	0.00282	2.6
141	6	1	6	13699.43457	13699.42833	0.00624	0.00768	0.8
141	6	2	5	13865.11253	13865.11778	-0.00525	0.00812	0.6
141	6	5	2	14444.96062	14444.94717	0.01345	0.00383	3.5
141	7	0	7	13828.24400	13828.25339	-0.00939	0.01948	0.5
141	7	1	6	13991.45999	13991.53176	-0.07177	0.00303	23.7

141	7	2	5	14097.35477	14097.20487	0.14990	0.02035	7.4
141	7	3	4	14207.65970	14207.65415	0.00555	0.00177	3.1
141	7	5	3	14612.91470	14612.92154	-0.00684	0.00161	4.2
141	8	1	8	13986.52807	13986.52151	0.00656	0.00400	1.6
141	9	0	9	14147.06489	14147.03636	0.02853	0.01687	1.7
141	9	2	8	14385.86500	14385.84613	0.01887	0.01596	1.2
141	9	3	7	14589.68295	14589.65716	0.02579	0.00288	9.0
141	10	0	10	14327.90837	14327.91388	-0.00551	0.00256	2.2
141	10	1	9	14592.95557	14592.96240	-0.00683	0.01089	0.6
141	10	1	10	14326.04690	14326.06596	-0.01906	0.01783	1.1
141	10	2	9	14596.59444	14596.57370	0.02074	0.02010	1.0
141	10	3	8	14816.87816	14817.01966	-0.14150	0.02006	7.1
141	11	0	11	14539.58275	14539.57761	0.00514	0.02009	0.3
141	11	1	10	14827.07398	14826.99386	0.08012	0.01546	5.2
141	11	1	11	14526.95617	14526.99823	-0.04206	0.02006	2.1
141	11	4	8	15286.82355	15286.81468	0.00887	0.00605	1.5
141	12	4	8	15615.08954	15615.08448	0.00506	0.00456	1.1
151	5	1	5	14993.42557	14993.41641	0.00916	0.00172	5.3
151	6	4	2	15743.96807	15743.98100	-0.01293	0.00147	8.8
160	5	4	2	13699.10540	13699.25584	-0.15044	0.00400	37.6
160	6	4	3	13843.65908	13843.67982	-0.02074	0.00400	5.2
160	7	4	3	14001.61338	14001.62130	-0.00792	0.01160	0.7
202	10	3	7	15663.43644	15663.28349	0.15295	0.00800	19.1
202	11	3	8	15917.63110	15917.78234	-0.12124	0.01593	7.6
211	13	5	9	14666.81259	14666.90389	-0.09130	0.01106	8.3
221	5	1	5	13964.26888	13964.27934	-0.01046	0.00141	7.4
221	9	0	9	14515.22882	14515.23621	-0.00739	0.00146	5.1
221	9	5	5	15209.29090	15209.32590	-0.03500	0.00135	25.9
221	10	2	9	14906.81997	14906.82798	-0.00801	0.00137	5.8
221	10	3	7	15170.40682	15170.41455	-0.00773	0.00154	5.0
221	10	6	4	15492.59150	15492.58205	0.00945	0.00225	4.2
221	11	3	8	15432.95004	15432.87246	0.07758	0.00250	31.0
221	11	3	9	15322.09606	15322.08766	0.00840	0.00185	4.5
221	11	4	7	15533.66938	15533.67609	-0.00671	0.00407	1.6
221	11	4	8	15478.60485	15478.61579	-0.01094	0.00475	2.3
221	12	3	9	15712.64820	15712.62942	0.01878	0.00402	4.7
221	12	4	8	15824.94570	15824.96738	-0.02168	0.00800	2.7
230	8	7	2	13769.04247	13769.03699	0.00548	0.00241	2.3
230	12	6	7	14539.76535	14539.75432	0.01103	0.00200	5.5
240	1	1	1	13262.58823	13262.56441	0.02382	0.00962	2.5
240	2	0	2	13272.81691	13272.82997	-0.01306	0.00217	6.0
240	2	1	1	13321.30669	13321.31542	-0.00873	0.00979	0.9
240	3	3	0	13639.98606	13640.01331	-0.02725	0.00192	14.2
240	4	0	4	13422.65508	13422.67093	-0.01585	0.00949	1.7
240	4	2	2	13586.74553	13586.75428	-0.00875	0.02807	0.3
240	4	2	3	13572.63757	13572.64369	-0.00612	0.00150	4.1
240	4	3	1	13734.66873	13734.65945	0.00928	0.00905	1.0
240	4	3	2	13734.48834	13734.48312	0.00522	0.00289	1.8
240	5	1	4	13627.21654	13627.24973	-0.03319	0.00164	20.2
240	5	1	5	13535.31707	13535.30939	0.00768	0.00203	3.8
240	5	3	3	13852.24934	13852.25772	-0.00838	0.00179	4.7
240	5	4	2	14050.06676	14050.05979	0.00697	0.00542	1.3
240	6	0	6	13641.86362	13641.92662	-0.06300	0.00310	20.3
240	7	4	3	14358.90385	14358.89165	0.01220	0.00481	2.5
240	8	2	7	14144.65501	14144.63141	0.02360	0.00185	12.8
240	8	5	4	14783.11388	14783.10079	0.01309	0.00451	2.9
240	9	1	8	14328.50713	14328.48542	0.02171	0.00400	5.4
240	9	1	9	14077.01224	14077.01862	-0.00638	0.00610	1.0
240	10	0	10	14281.41036	14281.48541	-0.07505	0.02920	2.6

240	10	2	9	14546.27525	14546.23089	0.04436	0.00300	14.8
240	11	5	6	15498.63182	15498.62685	0.00497	0.00134	3.7
301	10	2	8	15174.17602	15174.18157	-0.00555	0.00196	2.8
301	10	5	5	15387.31629	15387.32227	-0.00598	0.00257	2.3
301	10	6	5	15539.39900	15539.45451	-0.05551	0.03402	1.6
310	10	8	3	14327.72455	14327.73511	-0.01056	0.00250	4.2
310	12	5	8	14361.75280	14361.75923	-0.00643	0.01050	0.6
320	5	3	2	14169.56211	14169.56828	-0.00617	0.00179	3.4
320	5	3	3	14165.54696	14165.55371	-0.00675	0.00197	3.4
320	8	1	7	14503.33570	14503.34421	-0.00851	0.00298	2.9
320	9	1	8	14691.64169	14691.64744	-0.00575	0.00153	3.8
320	9	1	9	14505.65020	14505.75000	-0.09980	0.00200	49.9
320	9	2	8	14692.11426	14692.10793	0.00633	0.00128	4.9
320	10	0	10	14685.08406	14685.09097	-0.00691	0.00347	2.0
320	11	1	10	15120.97216	15120.97966	-0.00750	0.00239	3.1
320	11	3	9	15288.48318	15288.45722	0.02596	0.00500	5.2
400	9	2	8	14831.62146	14831.61298	0.00848	0.00400	2.1
400	9	5	4	15145.11020	15145.11809	-0.00789	0.00021	37.6
400	10	0	10	14864.64251	14864.65181	-0.00930	0.00401	2.3
400	11	1	10	15245.67413	15245.68661	-0.01248	0.00175	7.1
400	11	2	10	15246.74540	15246.75218	-0.00678	0.00914	0.7
400	11	8	3	16088.78318	16088.79303	-0.00985	0.00800	1.2
400	12	1	12	15276.93078	15276.95385	-0.02307	0.01235	1.9
400	12	3	10	15653.97103	15653.95120	0.01983	0.00300	6.6

Note

[a] $R = \frac{|This\ work - W2020|}{Unc W2020}$ is the ratio of the absolute deviation of the W2020 energy level value from the value derived from the present CRDS recordings by the corresponding W2020 uncertainty [18].

Conflict of Interest

The authors declare that they have no known competing financial interests or personal relationships that could have appeared to influence the work reported in this paper.

S. Vasilchenko: Investigation, **S.N. Mikhailenko:** Investigation, **A. Campargue:** Investigation